Atomic hydrodynamics of DNA: Coil-uncoil-coil transitions in a wall-bounded shear flow

William C. Sandberg[1,*] and Guan M. Wang[2,†]
[1]*Laboratory for Computational Physics and Fluid Dynamics, Naval Research Laboratory, Washington, DC 20375, USA*
[2]*Chemistry Division, Naval Research Laboratory, Washington, DC 20375, USA*
(Received 28 February 2008; revised manuscript received 18 August 2008; published 5 December 2008)

Extensive experimental work on the response of DNA molecules to externally applied forces and on the dynamics of DNA molecules flowing in microchannels and nanochannels has been carried out over the past two decades, however, there has not been available, until now, any atomic-scale means of analyzing nonequilibrium DNA response dynamics. There has not therefore been any way to investigate how the backbone and side-chain atoms along the length of a DNA molecule interact with the molecules and ions of the flowing solvent and with the atoms of passing boundary surfaces. We report here on the application of the nonequilibrium biomolecular dynamics simulation method that we developed [G. M. Wang and W. C. Sandberg, Nanotechnology **18**, 4819 (2007)] to analyze, at the atomic interaction force level, the conformational dynamics of short-chain single-stranded DNA molecules in a shear flow near a surface. This is a direct atomic computational analysis of the hydrodynamic interaction between a biomolecule and a flowing solvent. The DNA molecules are observed to exhibit conformational behaviors including coils, hairpin loops, and figure-eight shapes that have neither been previously measured experimentally nor observed computationally, as far as we know. We relate the conformational dynamics to the atomic interaction forces experienced throughout the length of a molecule as it moves in the flowing solvent past the surface boundary. We show that the DNA conformational dynamics is related to the asymmetry in the molecular environment induced by the motion of the surrounding molecules and the atoms of the passing surface. We also show that while the asymmetry in the environment is necessary, it is not sufficient to produce the observed conformational dynamics. A time variation in the asymmetry, due in our case to a shear flow, must also exist. In order to contrast these results with the usual experimental situation of purely diffusive motion in thermal equilibrium we have also carried out computations with a zero shear rate. We show that in thermal equilibrium there is asymmetry and an atomic hydrodynamic coupling between DNA molecules and the solvent molecules but there is no coil-uncoil transition.

DOI: 10.1103/PhysRevE.78.061910 PACS number(s): 87.15.ap, 34.35.+a, 47.11.Mn

I. INTRODUCTION

The use of nanometer-length DNA molecules in the newest functionalized-surface biosensor designs requires an understanding of how these short biomolecules behave in wall-bounded shear flows. There is currently no experimental means of investigating the atomic interaction-induced dynamics of molecules of this size, hence it was necessary to develop a computational method of investigation. A nonequilibrium biomolecular dynamics (NEBD) method was therefore developed and used to investigate the dynamics of short (10 nm) length-scale DNA molecules tethered to or flowing past surfaces with solvent explicitly involved [1,2]. The majority of previous investigations over the past two decades have focused on the response of micron-scale DNA molecules to thermal fluctuations of their equilibrium environment and to externally applied, single-direction stretching forces. Many optical experiments have been carried out to investigate the flow-induced transport of micron-sized DNA molecules [3–17], the deformation of tethered polymers [18], and the mobility of DNA in microchannels [19]. These results are not applicable to the new biosensor design issues due to the massive length and time-scale differences. Recently, experimental results have been obtained in nanochannels [20,21], however, the length scale of the molecules (microns) is still three orders of magnitude too large for our design purposes. Sotomayor and Schulten [23] reviewed *in vitro* and *in silico* experiments to probe the mechanical properties of biological matter, at the nanometer scale, but in equilibrium rather than in a shear flow. They point out that the experiments that have been carried out to date cannot, even in equilibrium, reveal the underlying atomic dynamics giving rise to the observed biomolecular responses. They therefore emphasize the importance of simulation experiments to provide insights into the possible causes for the experimental observations. Cohen and Moerner [22] discussed recent experimental work carried out to investigate, also in equilibrium, thermally driven shape fluctuations in double-stranded DNA. Their analysis of the experimental density-density correlations of individual molecules suggested to them the existence of a poorly understood radial structure and a hydrodynamic coupling, which they suggest may be weaker in their experiments than would occur in a free solution in equilibrium. They have no experimental means, however, of probing the existence of a hydrodynamic coupling. Recently several investigators have experimentally

*Present address: Science Applications International Corp., McLean, VA 22102, USA.
†Present address: George Mason University, Fairfax, VA 22030, USA.

explored the flexibility of short length-scale DNA dynamics, since flexibility plays such an important role in many cellular processes such as the packing of DNA in viruses [24–26]. Wiggins *et al.* [25] analyzed bending angle distributions in atomic force microscopy data and found spontaneous large-angle bends are far more prevalent in short length-scale DNA than predicted by classical DNA elastic models, which were developed to explain longer length-scale DNA data.

Computational investigations have also accompanied many of the previous long length-scale DNA experimental investigations. Brownian dynamics simulations have been carried out by many investigators to gain insights into the dynamics of long-chain polymers represented by micron-sized DNA molecules. Shaqfeh [27] has recently summarized much of this computational work. In Brownian dynamics, which is used most often for micron-scale DNA simulations, the molecules are represented by a bead and spring chain. Each bead represents tens or even hundreds of atoms. The response of the bead-spring system to the thermal equilibrium fluctuating forces of the solvent, or to applied steady external forces such as an elongational force on the molecule, is modeled. The model is either a linear or a nonlinear function of the extension of the chain from the equilibrium chain length. Hydrodynamic interaction forces due to the interaction of the bead-chain system with the solvent, if included, are also often modeled using low-Reynolds number continuum tensor formulations. However, as noted above, such models have been developed to explore dynamics at length and time scales that are far larger than the characteristic molecular lengths and times in our domain of interest. We require length and time resolution that existing computational models do not possess.

To explore the origin of nanometer-scale biomolecular conformational dynamics in a flow one must understand, at the atomic level, how the interactions between the constituent molecules of DNA, the flowing molecules and ions making up the biomolecular solvent, and the atoms of the bounding solid surfaces all contribute to the time-varying behavior of the flowing DNA molecules. Such atomic-level understanding is needed in order to assess the performance benefits of alternative biosensor designs and reduce problems associated with nonspecific binding, interactions between closely spaced wall-mounted biomolecules, agglomeration of near-wall biomolecules, and interference with near-wall transport. The existing experimental data on micron-sized single DNA molecules in equilibrium, or even in flows, is inherently incapable of providing answers to these questions.

In the work we report on here we have not used any models to represent the nanometer length-scale DNA molecules themselves, nor have we used any models to represent the response of the DNA molecules to the shear flow. We have extended our previous computations and analyze the conformational dynamics of each of the DNA molecules by directly computing the atomic interaction force and moment time histories between the atoms of the backbone and the side chains of each biomolecule and its time-varying local atomic environment. We computed, at each time step, the interaction between the flowing ions and water molecules of the moving ionic water solvent, the passing atoms of the wall surface, and the molecular constituents of each of the single-stranded DNA (ssDNA) molecules. This is a direct investigation of the time-varying atomic hydrodynamics, or coupling that Cohen and Moerner speculated might exist in their equilibrium system, but in our case, between DNA molecules and the solvent flowing past them in a wall-bounded geometry. We have, for the purposes of comparison, also computed the interaction between the DNA molecules and an equilibrium thermally fluctuating solvent. This enables us to inquire if there is an equilibrium hydrodynamic coupling, as speculated by Cohen and Moerner, and if there is, to see how it differs from nonequilibrium hydrodynamic coupling.

II. COMPUTATIONAL METHOD

The initial locations and orientations of six ssDNA molecules numbered from 1 to 6 in a computational box with a length, width, and height of 188, 94, and 120 Å, respectively, bounded by two gold atomic surfaces (walls) are shown. There are 107 047 atoms, including the water molecules, the 200 Na^+, and the 80 Cl^- ions.

The computational approaches for atomic molecular dynamics (MD) with shear flow that have appeared in literature can be classified into two broad categories: homogeneous shear methods [28–30] and boundary driven shear methods [31]. The first approach has found wide applications in the study of transport properties of homogeneous liquid, for example, the study of diffusion coefficients and a variety of auto- and cross-correlation functions [32,33] related to macroscopic transport coefficients, and the visualization of atomic liquid structural motion under shear flow [34]. In this work, we adopted the boundary driven methods in generating shear flow, i.e., translating the two walls in opposite directions. The homogeneous shear methods are not practical at high shear rates for our cases in that our systems, with either tethered or free macromolecules, are nonhomogeneous. There are different ensembles one can choose to carry out MD simulations. Since we are addressing cases with shear flows involved, velocity scaling is needed to maintain the desired temperature. Hence the constant number, volume, temperature (*NVT*) ensemble was chosen for all simulations.

The shear flow was built and maintained by moving the surface atoms at the box ends in opposite directions as shown in Fig. 1. The shear flow rate was on the order of $10^9\ s^{-1}$, which is typical of electro-osmotic flows in nanochannels [35]. The thermal temperature of the system was calculated based on the peculiar velocities, i.e., $V_x^{\text{peculiar}} = V_x - V_x^{\text{flow}}$, where V_x is the velocity in the x direction and the middle plane of the computational box is at $z=0$. The peculiar velocities in the y and z directions are counted as they are. V_x^{flow} is the local average velocity in the flow direction in a slab. Velocity scaling is performed on the peculiar velocities only. Velocity scaling is further confined to apply only to atoms of water molecules and ions. Three-dimensional periodic boundary conditions are used. Once a water molecule as a whole moves out from one side of the box, the "crystal" command in CHARMM brings the atoms back into the box through the opposite side. To perform MD simulations, the proper force field data are essential. The energy function in CHARMM is in general expressed as follows:

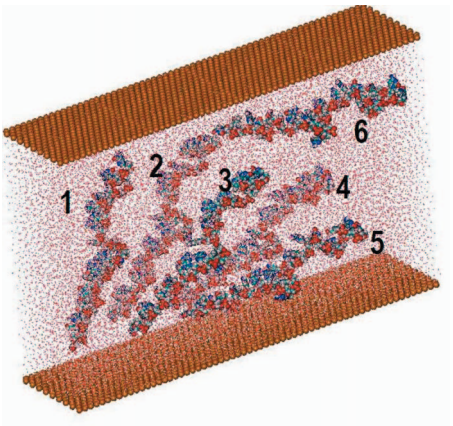

FIG. 1. (Color) Geometry of atomic Au nanochannel walls and initial position and orientation of the six DNA molecules surrounded by water molecules and ions.

$$U = E_{\text{bond}} + E_{\vartheta} + E_{\varphi} + E_{\omega} + E_{\text{elec}} + E_{\text{vdw}} + E_{\text{cons}} + E_{\text{other}}$$
$$= \sum k_b(b - b_0)^2 + \sum k_\theta(\theta - \vartheta_0)^2 + \sum [|k_\varphi| - k_\varphi \cos(n\varphi)]$$
$$+ \sum k_\omega(\omega - \omega_0)^2 + \sum_{i<j} \frac{q_i q_j}{4\pi\varepsilon_0 r_{ij}} + \sum_{i<j} \left(\frac{A_{ij}}{r_{ij}^{12}} - \frac{B_{ij}}{r_{ij}^{6}} \right) + E_{\text{cons}}$$
$$+ E_{\text{other}}.$$

Energy terms correspond, in order, to the potential of bond, bond angle, dihedral angle (torsion), improper torsion, electrostatic, van der Waals, constraint, and other term defined by users. Electrostatic and van der Waals potentials together are called nonbonded interactions. Detailed information on the assumptions and details of the potential functions are provided in the original paper by Brooks *et al.* [36]. For example, in the bond potential E_{bond}, k_b, and b_0 are the force field parameters, the force constant, and the equilibrium bond length, respectively. The cutoff distance was chosen as 14 angstroms in the calculations.

The initial structure (IS) of each DNA molecule in our computation is identical at each stage of construction of the computational supercell. For the purpose of consistency the IS was identical to the IS used (for the capture strand) in our previous paper [2]. The following steps describe the process that was used to generate the initial structure: (i) construct an actual experimentally used sequence of 21 base pairs by incorporating the helical structure parameters of a segment of a DNA chain from the DNA data bank; (ii) mechanically stretch the segment until the backbone is almost straight using CHARMM potentials, but without any solvent molecules or ions involved (the purpose of doing this is to simulate the random structure of short DNAs in biosensors); (iii) place one strand of the stretched structure in the solvent (water) with neutralizing ions and perform an energy minimization until the total potential energy converges; and (iv) perform an equilibrium MD simulation at room temperature for 20 ps with a time step of 1 fs by which time the structure is dynamically equilibrated. The resulting structure is the IS. The six DNA molecules in all supercells were formed from this IS by rotating and/or translating each of them to a position

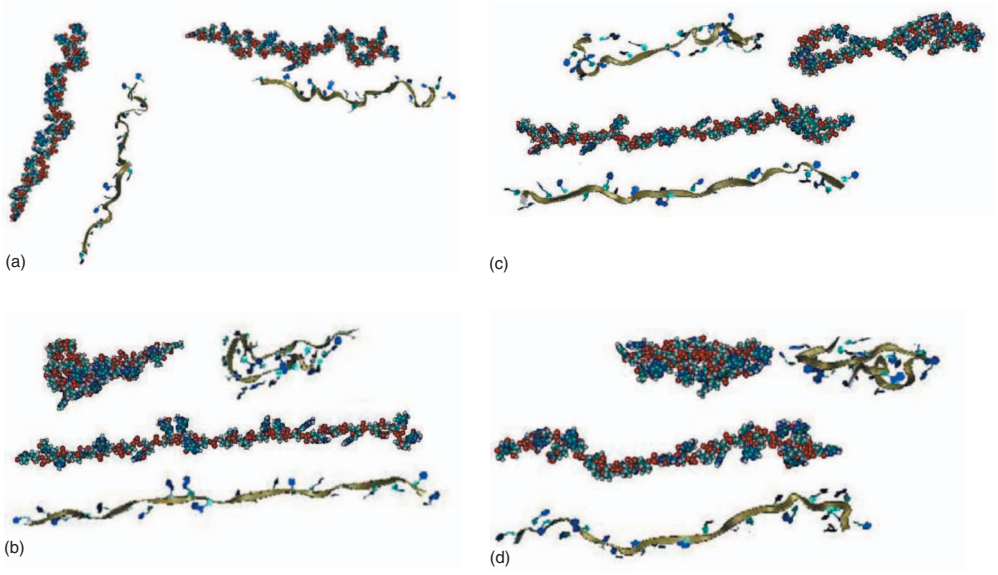

FIG. 2. (Color) Instantaneous molecular configurations of, and comparisons between, DNA molecule 6 (upper) and DNA molecule 1 (lower). Atomic representation shows the actual relative atomic positions while the ribbons show the backbone structures and blue dots are the attached bases. For clarity the water molecules and ions are not shown. (a) $t=0$ ps. Molecule 1 (left) is across the channel centerplane and molecule 6 (right) is adjacent to the wall. Both molecules had the same initially minimized, thermally equilibrated length. (b) $t=29$ ps. Molecule 1 has been rotated and stretched as it aligned with the flow. Molecule 6 has coiled into a hairpinlike configuration as it also aligned with the flow. (c) $t=53$ ps. Molecule 1 has remained in an extended configuration as it remains aligned with the flow direction. Molecule 6 has gone from a tightly coiled hairpinlike state to a figure-eight loop configuration, also remaining aligned with the flow direction. (d) $t=124$ ps. Molecule 1 has shortened slightly with some kinks but still is primarily aligned with the flow direction. Molecule 6 has compressed its length but retains the figure-eight configuration with a twist.

that would allow us to sample a range of locations with respect to the bounding surface and an orientation with respect to the wall. For each computational supercell, the six DNA molecules, together with solvent and surfaces, were then subjected to yet another energy minimization, and, following that, were again dynamically equilibrated in another equilibrium MD simulation for up to 10 ps at room temperature before beginning the shear flow simulations and recording any data on molecule extension, rotation, and coiling. Throughout the course of the energy minimization and thermal equilibration simulations none of the DNA molecules were observed to execute any drastic conformational changes such as those that were observed during the shear flow simulations. The end-to-end length of each DNA molecule remained close to 80 Å.

While initial states might be critical for final results in thermal equilibrium MD simulations, since the potential barriers may constrain the possible thermodynamic paths, that is not the case when a strong shear flow dominates. In the shear flow simulations the DNA molecules can easily overcome these potential energy barriers. As shown in our results, DNA molecules oriented perpendicular to the walls and located across the centerplane will initially respond with stretch and rotation whereas those DNA molecules initially near the walls and away from the zero-velocity center plane will respond with coiling-uncoiling transitions, regardless of the details of the minimized, thermally equilibrated initial structure.

We opted to follow the approach used by unified force field (UFF) modeling [37] and simulated the bounding gold nanosurfaces in a Lennard-Jones style model that was fitted to the Morse potential model of bulk gold [38]. Images of atoms in 26 mirror boxes within the cutoff distance were kept and updated for dynamics calculations. For all NEBD runs, the time step was 1 fs.

In this paper, many quantities are presented as smoothened over a time widow. In general, the smoothened function $\overline{f(t_i)|_w}$ of a function $f(t)$ of time with smoothening window width w is calculated as follows:

$$\overline{f(t_i)|_w} = \frac{\sum_{t_j \geqslant t_{\text{lower}}}^{t_{\text{upper}}} f(t_j)}{\sum_{t_j \geqslant t_{\text{lower}}}^{t_{\text{upper}}} 1}, \quad t_{\text{upper}} = \min(t_i + w/2, t_{\max}),$$

$$t_{\text{lower}} = \max(t_i - w/2, 0).$$

In the context, plotted $\overline{f(t_i)|_w}$ is marked by $f(t_i)$ for simplicity. Here f stands for any quantity that varies with time, including end-to-end length, radius of gyration, hydrodynamic force component, hydrodynamic torque component, and so on.

III. RESULTS AND DISCUSSION

A. DNA conformational dynamics in a shear flow

The conformational dynamics of each of the six DNA molecules has been computed throughout the course of our simulations. For clarity, we present only the results for molecules 1 and 6. The results obtained for molecules 2–5 are intermediate and bounded by those of 1 and 6, hence it is actually not necessary to present the details of the analysis for each of them, once we have examined in detail the behaviors of molecules 1 and 6. We observe in Fig. 2 that the conformational dynamics of molecules 1 and 6 evolve quite differently from each other. We will show below that this difference in conformational dynamics is due to the different time variation in the instantaneous atomic interaction force field that each bond, in each DNA molecule, is responding to. We also show below that the time variation in the interaction force field is itself due to the widely varying structure of each DNA molecules' instantaneous local environment due to its motion as it is advected by the shear flow. Quantitative measures of the changing molecular configurations are given by the time variation in the molecular end-to-end length and the time variation in the molecular radius of gyration as defined in the following:

End-to-end length:

$$L_{ee} = \sqrt{(x_2 - x_1)^2 + (y_2 - y_1)^2 + (z_2 - z_1)^2},$$

where (x_1, y_1, z_1) and (x_2, y_2, z_2) are the positions of the two oxygen atoms at the very ends of the backbone.

Center of mass:

$$x_c = \frac{\sum_{i=1}^{N} m_i x_i}{\sum_{i=1}^{N} m_i}, \quad y_c = \frac{\sum_{i=1}^{N} m_i y_i}{\sum_{i=1}^{N} m_i}, \quad z_c = \frac{\sum_{i=1}^{N} m_i z_i}{\sum_{i=1}^{N} m_i},$$

where N is the number of atoms in a DNA molecule, $N = 663$ in this paper.

Radius of gyration:

$$R_g = \sqrt{\frac{\sum_{i=1}^{N} m_i[(x_i - x_c)^2 + (y_i - y_c)^2 + (z_i - z_c)^2]}{\sum_{i=1}^{N} m_i}}.$$

The time-varying change in end-to-end length (L_{ee}) is shown for molecules 1 and 6 in Fig. 3(a) for the case of shear and in Fig. 3(b) for the case of diffusional motion only. The initial decrease, then increase, and then decrease in the end-to-end length of DNA molecule 6 is reflective of the coiled, uncoiled, and then coiled configurations, respectively, that are shown in Fig. 2. For molecule 1, the sudden increase in end-to-end length reflects the initial stretching experienced, prior to the subsequent rotation that is followed by length relaxation after the molecule has rotated sufficiently to align itself with the shear flow direction. DNA molecule 1 shows significant extension, approximately 200% of its equilibrium length, during the first 5 ps, immediately followed by a significant contraction, approximately 170% of its equilibrium length in the next 10 ps. The contraction in length is followed by a slow relaxation back to its equilibrium length after it has rotated to align itself with the flow direction.

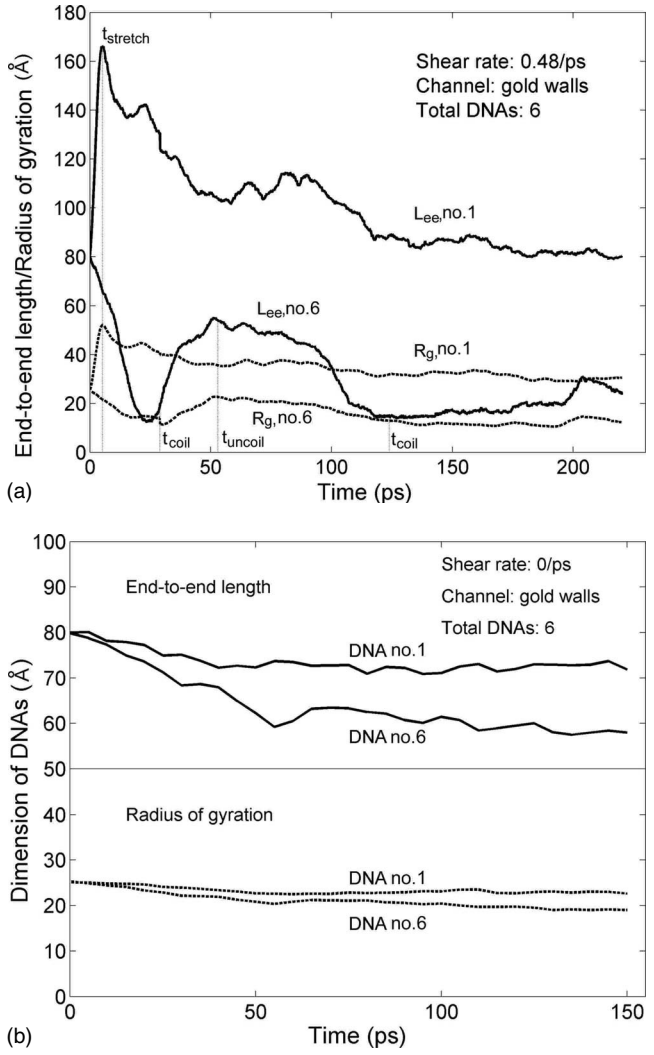

FIG. 3. (a) End-to-end length (L_{ee}) and radius of gyration (R_g) time variation of molecules 1 and 6 in a wall-bounded shear flow. Solid curves show L_{ee} variations of DNA molecules 1 and 6 and dotted curves show R_g variations. (b) End-to-end length (L_{ee}) and radius of gyration (R_g) time variation of molecules 1 and 6 in thermal equilibrium. Solid curves show L_{ee} variations of DNA molecules 1 and 6 and dotted curves show R_g variations.

There is no coiling or uncoiling behavior observed for molecule 1 during the entire simulation.

DNA molecule 6 on the other hand, immediately initiates such an extreme length *contraction* that its configuration totally changes, from a linear molecule to a compressed hairpin-shaped molecule, by around 29 ps, which is approximately ten times its natural relaxation period (as computed in [2]). DNA molecule 6 then proceeds to uncoil by around 50 ps, extending substantially and then again resumes coiling at about 100 ps. The instantaneous molecular conformations of DNA molecules 1 and 6 at these selected times are shown in Fig. 2. These conformational dynamics are totally unlike any experimental measurements to date for micron-sized DNA. Understanding the range of conformations taken by a biomolecule as it moves along the bounding substrate could be important in formulating a design strategy for new DNA-based nanoscale biosensors.

To emphasize the striking effects of a wall-bounded shear flow on DNA conformational dynamics, we compare them with the results from our equilibrium simulations. The initial conditions and the starting geometry for the equilibrium simulations are identical to that for the nonequilibrium case. The end-to-end length and radius of gyration time variation for the equilibrium results, shown in Fig. 3(b), show a very slowly varying, relatively flat pattern following the initial rotation and alignment. The slight differences between molecules 1 and 6 are due to the proximity of molecule 6 to the wall and its interaction with it. There is no indication of coiling and uncoiling behavior in either molecule. The embedding of the DNA molecules in a wall-bounded shear flow clearly results in a time-varying conformational evolution that is absent in the case of diffusional motion driven only by thermal fluctuations.

B. Total atomic collisional hydrodynamic force and torque time histories on DNA molecules in a shear flow

In order to attempt to understand why DNA molecules 1 and 6 had such drastically different conformational dynamics from the equilibrium results but also from each other in a shear flow, *after both had essentially aligned with the flow direction*, we investigated the detailed time-dependent atomic interaction forces experienced along the backbone and in the side chains of each molecule due to the time-varying solvent and bounding atomic gold nanosurface environment. We present first, since it is more easily understood, the time variation of the total hydrodynamic force (HF) and hydrodynamic torque (HT) components obtained by summing over the entire molecule. We then present the individual time-varying forces on each of the backbone and side-chain bonds along the molecule. The total molecular forces and torques for molecules 1 and 6 are computed as follows:

$$^{H}F_x = \sum_{i=1}^{N} f_{x,i}, \quad ^{H}F_y = \sum_{i=1}^{N} f_{y,i}, \quad ^{H}F_z = \sum_{i=1}^{N} f_{z,i},$$

$$^{H}T_x = \sum_{i=1}^{N} [(y_i - y_c)f_{z,i} - (z_i - z_c)f_{y,i}],$$

$$^{H}T_y = \sum_{i=1}^{N} [(z_i - z_c)f_{x,i} - (x_i - x_c)f_{z,i}],$$

$$^{H}T_z = \sum_{i=1}^{N} [(x_i - x_c)f_{y,i} - (y_i - y_c)f_{x,i}].$$

Instantaneous torque values with respect to the center of mass were obtained from instantaneous coordinates of, and forces on, each of the atoms of the backbone and side chains of each DNA molecule. The values shown in the plots have been smoothed by averaging over a window of 5 ps. These are plotted in Figs. 4 and 5 and compared with the results from the equilibrium simulations. Instantaneous torque values with respect to the center of mass were obtained from instantaneous coordinates of, and forces on, each of the at-

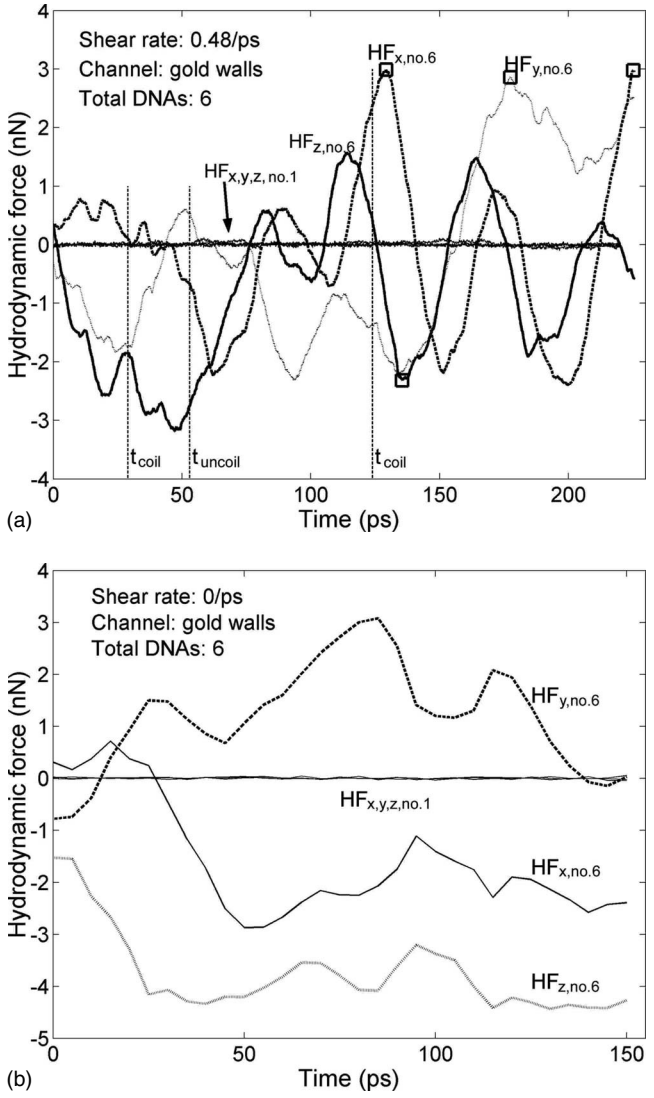

FIG. 4. (a) Total hydrodynamic force components on DNA molecules 1 and 6 as a function of time at a flow shear rate of 48 ps. (b) Total hydrodynamic force components on DNA molecules 1 and 6 as a function of time in an equilibrium solvent.

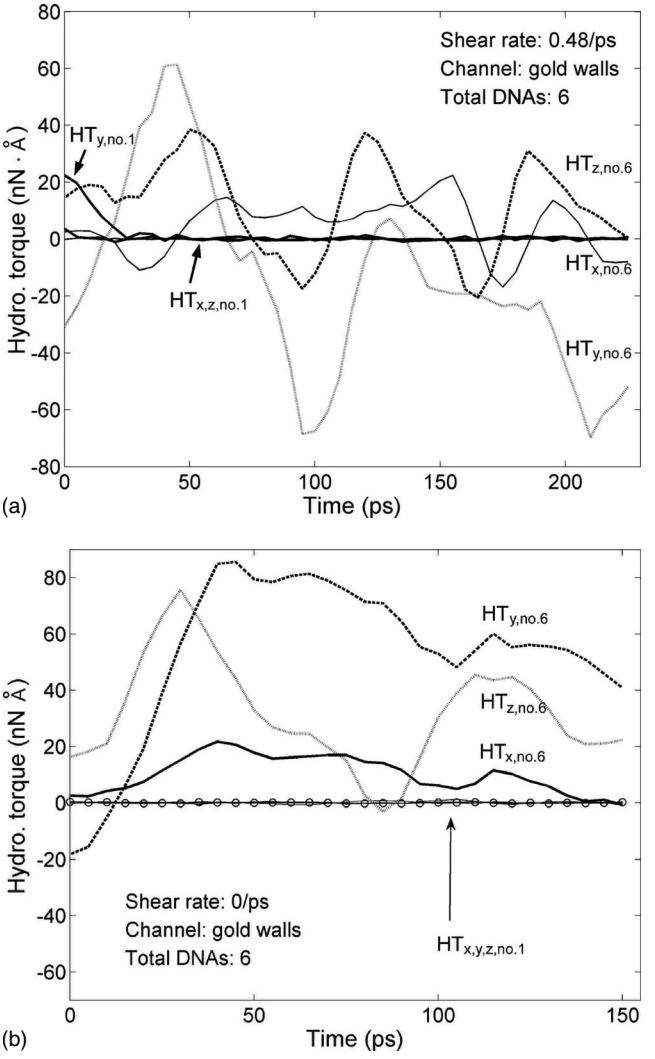

FIG. 5. (a) Total hydrodynamic torque components with respect to the center of mass of DNA molecules 1 and 6 as a function of time. (b) Total hydrodynamic torque components with respect to the center of mass of DNA molecules 1 and 6 as a function of time for the equilibrium case.

oms of the backbone and side chains of each DNA molecule. The values shown in the plots have been smoothed by averaging over a window of 5 ps.

It is clear from the comparison of Fig. 4(b) with Fig. 4(a) that the rapid time variation in the magnitude of the force components is substantially less for the equilibrium case. There is absolutely no variation for molecule 1, indicating that its environment remains essentially symmetric. The force time variation for molecule 6 is the result of the time-varying asymmetry in its environment as it diffuses near the wall.

The subscripts x, y, and z correspond to three perpendicular directions: x in the flow direction, z in the normal direction to the wall, and y perpendicular to the above two. Subscripts 1 and 6 denote DNA molecules 1 and 6. Very large variations in the magnitude and the direction of force and torque are observed acting upon DNA 6 throughout the shear flow simulation. The points marked with a square are the maxima in the force components on DNA molecule 6. Analysis of the variation in the distance between any two DNA molecules was carried out and showed that the time of occurrence of the maxima correspond to those times when DNA molecules 2, 3, 4, or 5 are close to DNA molecule 6, especially when one of them gets very close to it. For example, these peaks (squares) originated from the strong interaction (collisions) between DNA molecules 3 and 6. We observe from Fig. 4(a) that the positive, negative, and then positive regions of the x component of hydrodynamic force on DNA molecule 6 occur during the periods of coiling, uncoiling, and recoiling, as indicated on the time axis and are consistent with the coil-uncoil-coil dynamics shown in Fig. 2. This consistency is particularly striking during the first uncoiling event at $t \sim 55$ ps and the second coiling event at $t \sim 125$ ps. No such oscillatory behavior is observed in Figs. 4(b) and 5(b) for the equilibrium case, although the magnitude of the maximum force and torque are similar. The force magnitudes on DNA molecule 1 are on the order of 0.01 nN,

or about 2 to 3 orders of magnitude smaller than the force components on molecule 6. The torque components, HT_x and HT_z on DNA molecule 1 remain, throughout the simulation, on the order of 1 nN Å, or about 2 orders of magnitude smaller than those on molecule 6 for both the shear flow and the equilibrium simulation. This reduction in the magnitudes of the forces on molecule 1 compared to those on molecule 6 is a reflection of the symmetry in the environment of molecule 1. The essentially symmetric environment experienced by molecule 1 leads to a net cancellation of the total force. No such cancellation occurs with the complete lack of symmetry in the atomic environment of molecule 6. Molecule 6 is bounded on one side by the atomic wall and on the other side it is interacting with several of the other four passing DNA molecules. In addition, the solvent water molecules and ions flowing past molecule 6 are moving according to the imposed gradient, at different velocities, hence inducing rotation. For the equilibrium case we do observe in Fig. 5(b) that there is significant time variation in the torque magnitudes on molecule 6. This suggests that interactions among the six biomolecules and the wall are a major factor in the origination of the molecular torque time histories. If this is correct then we would expect a decrease in torque magnitude as the biomolecular concentration is decreased.

We next probe deeper into the individual atomic interaction force time histories experienced at *each base pair* along the backbone and in the side chains of each DNA molecule that gives rise to these integrated total values to see, if we can, how each structural entity along the length of DNA molecules 1 and 6 responds to the solvent environment as it passes by them, and the wall environment as they each pass by it. There is no experimental ability to make such an investigation; yet it is the time variation in the interaction force field between each base pair and its moving, changing environment that is ultimately responsible for the biomolecular response dynamics.

C. DNA molecular bonding force time histories in a shear flow

Internal molecular bonding force time histories have been computed along the backbone and between side chains and the backbone of both DNA molecules 1 and 6, in addition to the other four DNA molecules, as they are advected along and interact with the molecules and ions of the solvent in the shear flow, with each other, and with the passing atoms of the wall. Due to the complexity of the plot of the force time history of all backbone and all side-chain bonds, we provide below the results for only DNA molecules 1 and 6 in order to show how they relate to the conformational dynamics of those molecules. Following the CHARMM topology file notation, the backbone bond that was selected for force calculation is between O3′ from the sugar and P from the phosphate group; those side-chain bonds are between C1′ from sugar and either N1 (A, C bases) or N9 (G, T bases). Bonding forces were calculated from the instantaneous positions of the two ending atoms as follows:

$$^{B}F(t) = 2k_b[b(t) - b_0],$$

where k_b is the bond force parameter, which is 1129.68 and 920.48 kJ/mol (or 270 and 220 kcal/mol in the CHARMM database) for backbone bonds and side-chain bonds, respectively; b_0 is the equilibrium bond length, that is 1.6, 1.456, and 1.458 Å corresponding to bonds O3′–P, C1′–N1, and O3′–N9, respectively; and $b(t)$ and $^{B}F(t)$ are the instantaneous bond length and bonding force. Over the duration of most of our MD simulations, the backbone bonds tend to contract. That is, the values are between 0 and ~−2 nN with the average of −1 nN over 20 of them, which corresponds to a 0.11% backbone bond contraction. However, for DNA molecule 1 the backbone bonding force is particularly large in the initial DNA stretching stage. This is consistent with the initial large increase in the end-to-end length observed in Fig. 3. In addition, while many backbone bonds in the middle of the chains are stretched the most, there are a few bonds at the two ends of the chains that are only moderately stretched. DNA molecule 6 does not experience drastic bond stretch at the initial stage of the simulation. This is consistent with the fact that DNA molecule 6 was initially parallel to the flow while molecule 1 was nearly perpendicular to the flow with its middle point in the zero-velocity plane of the shear flow, which lead molecule 1 to the initial maximum stretch and concurrent rotation required to align with the flow direction. DNA molecule 6, after 50 ps, is interacting with DNA molecules 3, 4, and 5, hence there is substantial variation in the forces due to the increasing asymmetry of its environment. We observe substantial variability in time for the bonding force all along the backbone and at the side chains. There are prominent maxima apparent in the backbone bonding forces at the time for initial stretch of DNA molecule 1, seen clearly in Fig. 6(a), and at both the coiling and uncoiling times for DNA molecule 6, as can be easily seen in Fig. 6(b).

The backbone bonding forces of both DNA molecules fluctuate in a similar way and mostly within the typical range of between −2 and 0 nN. The side-chain bonding forces are also fluctuating and mainly between 0 and 1.2 nN for both DNA molecules. There are systematic stretches (in backbone bonds) and contractions (in side-chain bonds) observed, both on the order of 0.1% of the equilibrium bond length. The individual bond force time histories are observed to be consistent with the total molecule force time histories discussed above, thus demonstrating that the computed conformational dynamics of these two DNA molecules are consistent with the bond force time-history variation along the length of each molecule itself. Each bond force time-history variation, as one moves along the length of the molecule is, in turn, due to its own time-varying atomic environment.

We also observe, from Fig. 6 taken in conjunction with Fig. 2, that typical classical rheological bead-chain polymer representations combined with linear and nonlinear spring, bead-chain hydrodynamic response models are not directly comparable to the atomic interaction-induced bond level dynamics and resulting molecule conformational dynamics, which we have computed. The time-varying bond level dynamics of each particular bond is the local response of *that bond* to its *own* time-varying environment and this is fundamentally why *each* DNA molecule in the system has its own unique conformational dynamics. Polymer phenomenological models, since they were developed to describe rheologi-

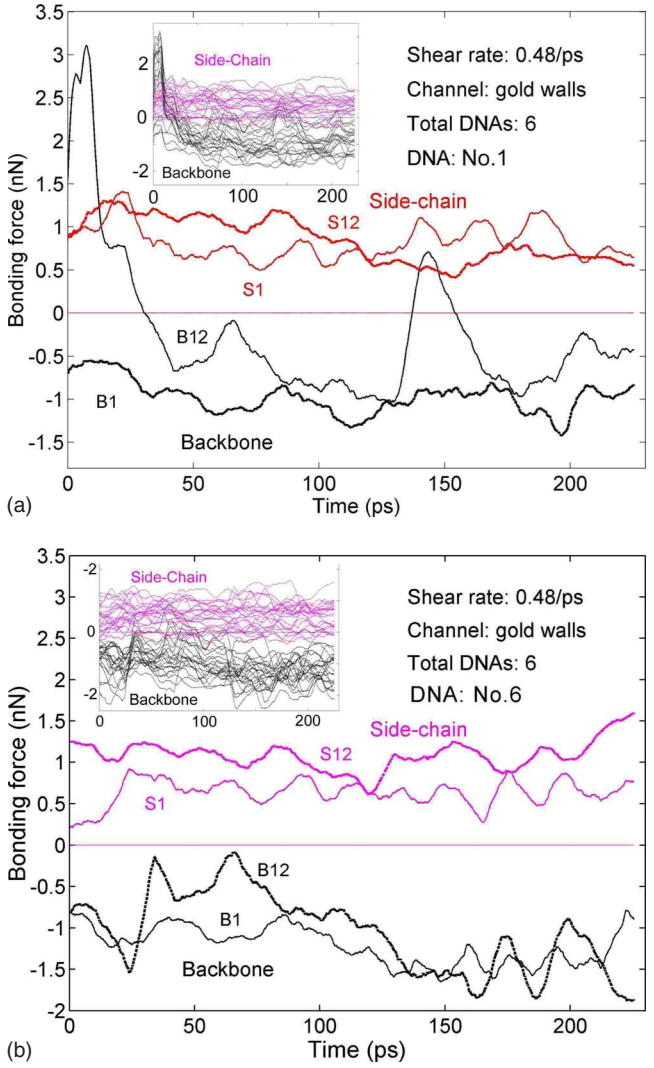

FIG. 6. (Color online) Internal bonding forces as a function of time in a shear flow for (a) DNA molecule 1 and (b) DNA molecule 6. B1 and B12 correspond to the first (end) and 12th (middle) backbone O–P bonds; S1 and S12 are the first and 12th (middle) sidechain-backbone bonds. Insets: Dark (black online version) curves are 20 backbone bonds and light (purple online) curves are side-chain bonds connecting them to the molecule backbone. (a) DNA molecule 1 bond force time-histories. (b) DNA molecule 6 bond force time histories.

cal flow behavior, are not capable of interrogating the flow at atomic length and time scales. A general continuum representation is therefore inherently incapable of describing unique individual bond dynamics. The reverse is not true, however, it is computationally not yet possible to use an atomic interaction force model to compute the dynamics of micron-sized DNA molecules in a continuum flow.

D. Effects of time-varying local atomic environment on DNA conformational dynamics

We carried out several additional simulations to successively isolate, if possible, the relative importance of each aspect of the time-varying environment of DNA molecule 6

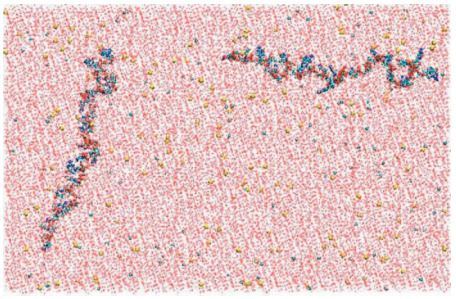

FIG. 7. (Color) Equilibrium MD simulation without walls for DNA molecules 1 and 6.

to its computed conformational dynamics. We examined first the role of the thermal motion of the solvent by carrying out the complete simulation with all molecules and the wall, but at zero shear, to remove the effects of the solvent shear flow. These results were discussed above where it was apparent that there was no evidence of coiling and uncoiling dynamics. As we noted above, the total force and torque components for molecule 6 for zero shear are of the same order of magnitude as for the shear flow case but do not exhibit the alternating positive and negative regions associated with the coil-uncoil-coil conformational dynamics. In the shear flow case, DNA molecule 6 is moving with the flow and periodically is passed by other DNA molecules since there is a velocity gradient in the channel. Hence DNA molecule 6 is subjected to oscillating changes in the forces and torques, especially in direction. That is, the absolute magnitude of the atomic interaction force at any given instant is *not* increased by increasing the velocity of the water molecules past the DNA molecule (since at any given instant the local atomic number density about a given molecule is not substantially different); but, the *time variation* of the force component magnitudes on the DNA molecule *are* increased as the flow is sheared, since the asymmetry of a DNA molecule's local environment is changing substantially over that experienced due only to thermal fluctuations. We conclude, from com-

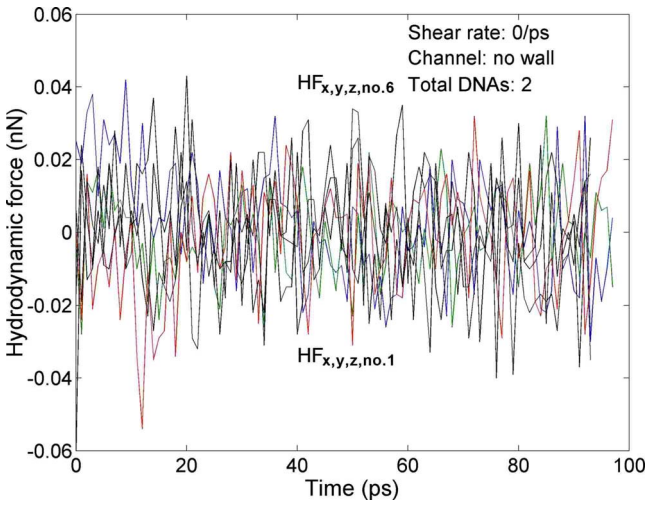

FIG. 8. (Color online) Total hydrodynamic force on only DNA molecules 1 and 6 as a function of time from equilibrium MD simulations without walls.

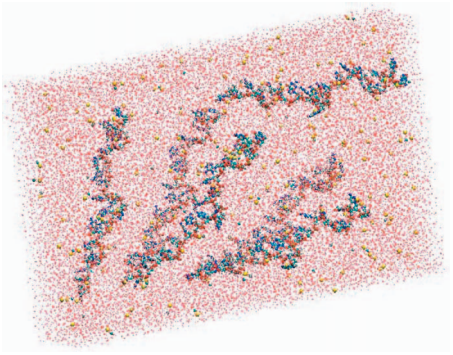

FIG. 9. (Color) Equilibrium MD simulation for six DNA molecules in a box without solid walls.

parisons of the force component time histories, that it is the time variation in the forces, particularly along the direction of the flow and in the direction normal to the wall, that is important for the occurrence of the coil-uncoil-coil behavior of molecule 6. As the shear rate increases, the interactions

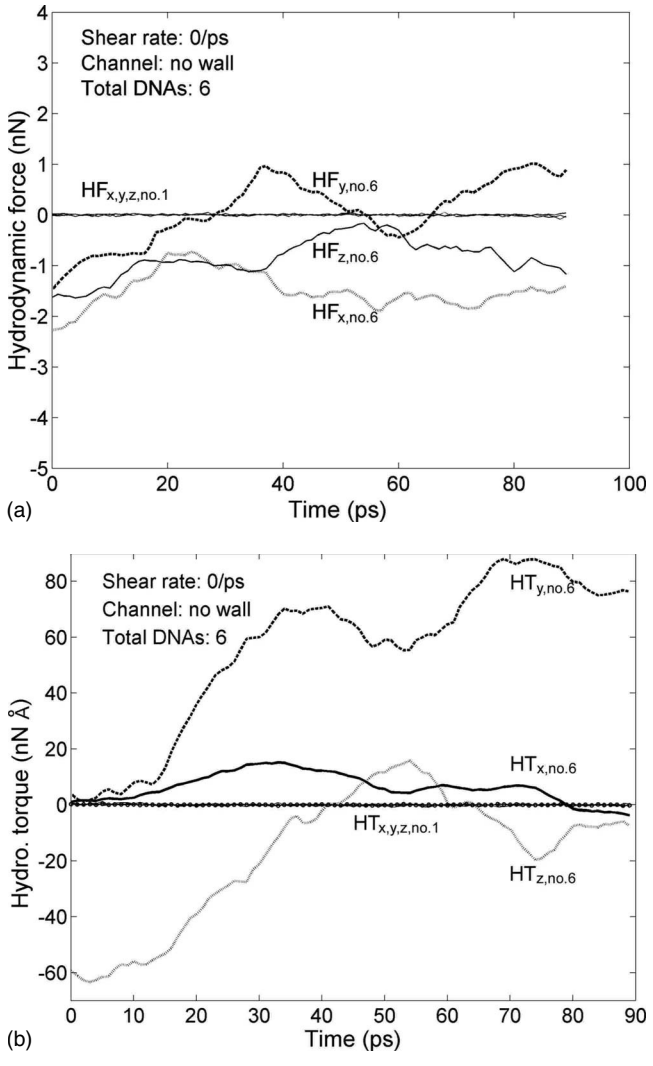

FIG. 10. (a) Total hydrodynamic force and (b) torque components of DNA molecules 1 and 6 as a function of time from equilibrium MD simulations without walls.

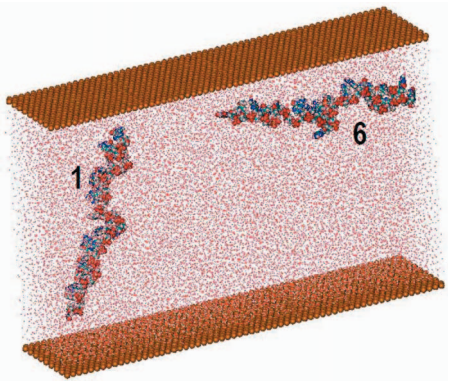

FIG. 11. (Color) NEBD simulation box with moving walls and the same initial locations and configurations of DNA molecules 1 and 6 as in Fig. 1.

among other passing DNA molecules will also increase, hence environmental symmetry will be lost for all DNA molecules. We therefore expect, for higher shear rates and longer run times, to see significant conformational variations for all of the DNA molecules. We also expect, for decreasing shear rates, that the time interval between coiling and uncoiling will progressively increase until finally, at zero shear, it will not be observed, even for molecule 6. We have confirmed this zero shear expectation by extending the equilibrium MD simulation to continue through 150 to 230 to 320 ps. We showed above in Figs. 3(a) and 3(b) the results for molecules 1 and 6 out to 150 ps and beyond. They do not change as the run continues to 320 ps. Only DNA molecule 6 exhibits any substantial conformational changes, eventually taking on an "S-like" shape that appears to be stable as the simulation continues, but with no observed coiling behavior.

Thus, from our computations, it appears that in thermal equilibrium there is insufficient asymmetry-induced time variation in the magnitude and direction of the interatomic forces to induce oscillatory conformational changes in any of the six DNA molecules. A shear flow is necessary.

We have compared the results for a shear flow with the force and torque time histories with all six DNA molecules and a wall in thermal equilibrium and observed no coiling or uncoiling behavior in equilibrium. We next inquire how these results change if we remove the four DNA molecules close to molecule 6 and also remove the wall. That is, we will now tear down the system and then sequentially build it back up, from the most primitive case to the most complex wall-bounded shear flow case, in order to assess the importance of each contribution. We examine first the most primitive situation of two DNA molecules, with no nearby surfaces, in water at zero shear. Since the other four DNA molecules have been removed we also removed a sufficient number of ions to maintain a neutral solution. The number of ions was changed to 160 Na^+ and 120 Cl^- to keep the system neutral and also to keep the total number of ions (280) the same as in the above cases. The physical situation for this case is shown in Fig. 7.

By removing DNA molecules 2–5, and the wall, the total hydrodynamic force and torque (not shown) on molecules 1 and 6 were reduced to a negligible level of ± 0.03 nN and

±1 nN Å, respectively, as observed in Fig. 8. This indicates the important contribution made by nearby molecules and the bounding substrate on the instantaneous force magnitude.

We proceed to build the system back up by next adding in the other four DNA molecules, but leaving out the wall and leaving out the shear flow. The physical situation is shown in Fig. 9.

Total force and torque components are plotted in Fig. 10 as a function of time. We observe that force component magnitudes are reduced by more than half if compared with the results of equilibrium simulations for channels with interacting atomic walls [shown in Fig. 7(a)], while the torque magnitudes are merely changed. This suggests that interacting atomic walls and the proximity of other DNA molecules will considerably impact the DNA translational motion, while the neighboring DNA molecule interactions taken alone without the walls included primarily effect the DNA rotation. This is reasonable since the asymmetrical charge distribution of strongly negatively charged DNA molecules is expected to interact electrostatically to impact DNA rotation as two DNA molecules move past one another. In thermal equilibrium there thus does exist a hydrodynamic "coupling," as speculated by Cohen and Moerner [22], between the molecules of the solvent and the DNA molecules. The magnitude of the coupling is dependent on the proximity of other DNA molecules in the solvent and the proximity of atomic surfaces.

The wall interaction forces are clearly extremely important to creating an asymmetrical local environment for each bond along the length of a DNA molecule. We finally examine the role of the shear flow itself created by moving the wall, but without the presence of the other four interacting DNA molecules. That is, we are asking if the interacting atomic wall itself and the shear flow its motion creates are sufficient to produce the coiling-uncoiling-coiling behavior in molecule 6 observed in the complete wall-bounded shear flow simulations. The physical situation is shown in Fig. 11.

The radius of gyration and end-to-end length time variation are observed, in Fig. 12, to closely resemble the results computed for the complete system of six interacting DNA molecules in a shear flow (shown in Fig. 3). This indicates that a shear flow and a nearby bounding atomic wall are sufficient, without additional DNA molecule interactions, to cause the coiling, uncoiling, and recoiling dynamics in DNA molecule 6. We observe that there is a factor of 4 reduction in end-to-end length occurring for molecule 6 within approximately 20 ps followed by an extension, which continues to reach a factor of 6 over the next 40 ps. The molecule relaxes and then executes another coiling, reducing its end-to-end length by approximately half of its starting value. The corresponding total hydrodynamic force components are plotted in Fig. 13. The force component $HF_{x,\text{no. }6}$ in the flow direction of the near wall DNA molecule 6 is the "pure" hydrodynamic force, in the range of 0.05–0.15 nN, and, as shown in Fig. 12, is capable of producing the drastic conformational changes observed in DNA molecule 6 if the molecule is moving past an atomically interacting wall. The dominance and time variation of the magnitude of force in the flow direction for the near-wall molecule is evident in Fig. 13.

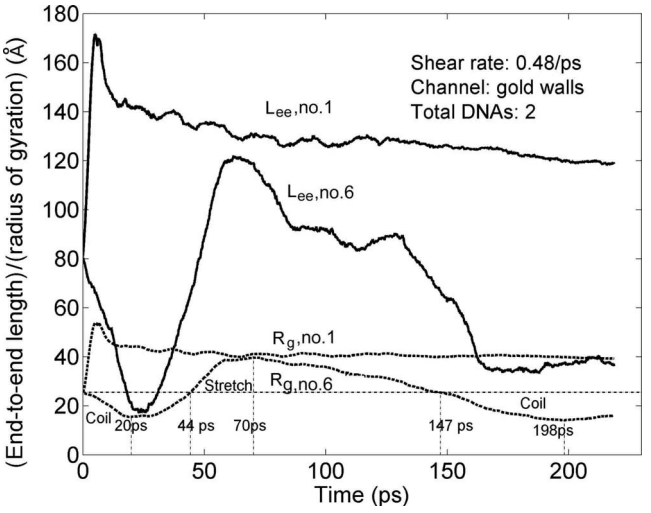

FIG. 12. Radius of gyration and end-to-end length of DNA molecules 1 and 6 as a function of time from NEBD simulations at a shear rate 0.48/ps with walls.

IV. CONCLUSIONS

A rich assortment of conformations has been computed for a 10 nm DNA molecule flowing past an atomic wall in an ionic water solvent. Coiling-uncoiling-coiling transitions occurred with hairpin and figure-eight loop configurations also observed. Other DNA molecules in the system exhibited conformational dynamics that varied from stretch relaxation to those approaching the coiling-uncoiling dynamics of the near-wall molecule. The dynamic behaviors of the nanometer length-scale DNA molecules in the shear flow simulations were found to have a sensitive dependence upon the instantaneous local atomic environment of each bond along the length of each molecule. The local atomic bond environment of each molecule varies in time differently depending upon how the molecule is oriented in the solvent flow, how many other DNA molecules are passing by it, and whether or not it

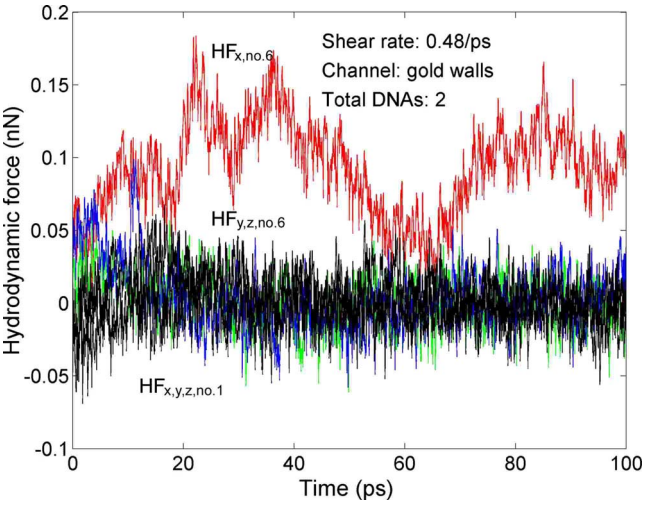

FIG. 13. (Color online) Total hydrodynamic force components on DNA molecules 1 and 6 as a function of time from NEBD simulations with walls at a shear rate of 0.48/ps.

is passing in proximity to any surfaces it can interact with. We have demonstrated that the computed conformational dynamics of the DNA molecules are consistent with the computed time variation of the total hydrodynamic force and torque on the molecules and also are consistent with the time variation of the backbone and side-chain bonding forces along the molecule length. We have found that the bonding forces are *not* constant along the backbone and at the connections between the backbone and side chains in a stable shear flow. Bonding forces may be up to several nanonewtons when DNA is highly stretched, with the maximum occurring in the middle portion and less at the two ends.

Total hydrodynamic forces and torques were observed to change often, both in direction and magnitude, along the length of each of the six DNA molecules during the simulation period of hundreds of picoseconds. From the results for only two DNA molecules in a shear flow above a wall, where the DNA-DNA interaction is disabled by sufficient separation, the drastic conformational behavior of successive coiling and uncoiling is still observed. This observation leads us to conclude that the dynamic conformational behavior of molecule 6, the near-wall molecule, is due to the time-varying asymmetry induced along its length by the shear flow caused by the motion of the wall. This behavior is not observed if there is no shear flow.

These results indicate that by properly orienting DNA molecules in a sheared solvent in a wall-bounded flow, very diverse conformational dynamics and resulting biomolecular physical properties of interest can be achieved. It would be interesting for future investigations to assess how sensitive these findings are to a variation in molecular interaction parameters such as would be caused by changing the composition of the solvent and by tailoring atomic-structural variations and associated charge distributions into the bounding wall itself. A separate investigation of interest would be to examine how the conformational dynamics of the DNA molecules in the system we have studied modify near-wall transport and how the modification of near-wall transport affects continuum flow away from the wall. These are particularly relevant questions for the design of biomolecular microdevices and tailored nanosystem flow sensors.

ACKNOWLEDGMENTS

W.C.S. and G.M.W. thank Lloyd J. Whitman, Jack Rife, and Shawn P. Mulvaney from the Chemistry Division at NRL for informative communications. All computation and simulations were performed on NRL High Performance Computer facilities through a grant from the DOD High Performance Computing Modernization Office. This work was supported by the Joint Science and Technology Office for Chemical and Biological Defense at the Defense Threat Reduction Agency (DTRA).

[1] G. M. Wang, W. C. Sandberg, and S. D. Kenny, Nanotechnology **17**, 4819 (2006).
[2] G. M. Wang and W. C. Sandberg, Nanotechnology **18**, 135702 (2007).
[3] S. B. Smith, L. Finze, and C. Bustamante, Science **258**, 1122 (1992).
[4] T. Perkins, D. E. Smith, and S. Chu, Science **264**, 819 (1994).
[5] T. T. Perkins, S. R. Quake, D. E. Smith, and S. Chu, Science **264**, 822 (1994).
[6] A. V. Vologodski, Macromolecules **27**, 5623 (1994).
[7] J. Marko and E. Siggia, Macromolecules **28**, 8759 (1995).
[8] T. T. Perkins, D. E. Smith, R. G. Larson, and S. Chu, Science **268**, 83 (1995).
[9] T. T. Perkins, D. E. Smith, and S. Chu, Science **276**, 2016 (1997).
[10] D. E. Smith and S. Chu, Science **281**, 1335 (1998).
[11] D. E. Smith, H. P. Babcock, and S. Chu, Science **283**, 1724 (1999).
[12] J. C. Meiners and S. R. Quake, Phys. Rev. Lett. **84**, 5014 (2000).
[13] C. Bustamante, S. B. Smith, J. Liphardt, and D. Smith, Curr. Opin. Struct. Biol. **10**, 279 (2000).
[14] P. S. Doyle, B. Ladoux, and J. L. Viovy, Phys. Rev. Lett. **84**, 4769 (2000).
[15] R. M. Robertson, S. Laib, and D. E. Smith, Proc. Natl. Acad. Sci. U.S.A. **103**, 7310 (2006).
[16] Y. C. Chung, Y. C. Liu, Y. L. Hsu, W. N. T. Chang, and M. Z. Shiu, J. Micromech. Microeng. **14**, 1376 (2004).
[17] R. Shusterman, S. Alon, T. Gavrinyov, and O. Krichevsky, Phys. Rev. Lett. **92**, 048303 (2004).
[18] Y. Gratton and G. W. Slater, Eur. Phys. J. E **17**, 455 (2005).
[19] P. J. Shrewsbury, S. J. Muller, and D. Liepmann, Biomed. Microdevices **3**, 225 (2001).
[20] D. Stein, F. H. van der Heyden, W. J. A. Koopmans, and C. Dekker, Proc. Natl. Acad. Sci. U.S.A. **103**, 15853 (2006).
[21] J. D. Cross, E. A. Strychalski, and H. G. Craighead, J. Appl. Phys. **102**, 24701 (2007).
[22] A. E. Cohen and W. E. Moerner, Phys. Rev. Lett. **98**, 116001 (2007).
[23] M. Sotomayor and K. Schulten, Science **316**, 1144 (2007).
[24] P. K. Purohit, J. Kondev, and R. Phillips, Proc. Natl. Acad. Sci. U.S.A. **100**, 3173 (2003).
[25] P. A. Wiggins, T. van der Heijden, F. Moreno-Herrero, A. Spakowitz, R. Phillips, J. Widom, C. Dekker, and P. C. Nelson, Nat. Nanotechnol. **1**, 137 (2006).
[26] T. Cloutier and J. Widom, Mol. Cell **14**, 355 (2004).
[27] E. S. G. Shaqfeh, J. Non-Newtonian Fluid Mech. **130**, 1, (2005).
[28] S. Kumar and D. Giri, Phys. Rev. Lett. **98**, 048101 (2007).
[29] D. J. Evans and G. P. Morriss, Phys. Rev. A **30**, 1528 (1984).
[30] D. J. Evans and G. P. Morris, *Statistical Mechanics of Nonequilibrium Liquids* (Academic, London, 1990).
[31] W. C. Sandberg and D. M. Heyes, Mol. Phys. **85**, 635 (1995).
[32] D. M. Heyes, J. Chem. Phys. **85**, 997 (1986).
[33] D. M. Heyes, *The Liquid State: Applications of Molecular Simulations* (Wiley, Chichester, 1997).

[34] W. C. Sandberg, U. Obeysekare, C. Williams, and A. Qasba, Phys. Chem. Liq. **35**, 67 (1997).
[35] D. Kim and E. Darve, Phys. Rev. E **73**, 051203 (2006).
[36] B. R. Brooks, R. E. Bruccoleri, B. D. Olafson, D. J. States, S. Swaminathan, and M. Karplus, J. Comput. Chem. **4**, 187 (1983).
[37] A. K. Rappé, C. J. Casewit, K. S. Colwell, W. A. Goddard III, and W. M. Skiff, J. Am. Chem. Soc. **114**, 10024 (1992).
[38] R. C. Lincoln, K. M. Koliwad, and P. B. Ghate, Phys. Rev. **157**, 463 (1967).